Journal of Sound and Vibration (1999) **221**(1), 23–47
Article No. jsvi.1998.2012, available online at http://www.idealibrary.com.on IDEAL

ATTENUATION OF CAVITY FLOW OSCILLATION THROUGH LEADING EDGE FLOW CONTROL

X. Zhang, X. X. Chen and A. Rona

Department of Aeronautics and Astronautics, University of Southampton, Southampton SO17 1BJ, England

AND

J. A. Edwards

Weapons Systems Sector, DERA, Fort Halstead, Sevenoaks, Kent TN14 7BP, England

(*Received* 28 *July* 1998)

The unsteady flows over a shallow rectangular cavity at Mach 1·5 and 2·5 are modified at the leading edge by using compression ramps, expansion surfaces, and mass injection. The study is performed through solutions of Short-time Reynolds-Averaged Navier–Stokes equations (TRANS) with turbulence modelled by a two-equation k–ω model. When a compression ramp is introduced, two types of responses are observed: at Mach 1·5, a strong flapping motion leads to small changes in the frequency and sound pressure level in the cavity compared with the baseline case of rectangular geometry. The roll-up of the shear layer produces convective vortices, leading to enhanced pressure fluctuations on the downstream surface; At Mach 2·5, a weak shear layer instability produces a reduction in the sound pressure level, and the increased distance between the leading edge and the trailing edge produces a reduction in frequency. An increase in the mean pressure drag coefficient is produced due to the high pressure on the ramp. When an expansion surface is employed, the mean pressure drag coefficient is also increased slightly. When the flow is attached to the surface, the major flow physics are similar to the baseline case. A reduction of the sound pressure level is observed in the cavity with the surface height. When a shock induced separation occurs on the surface, a steady flow is established in the cavity. When the mass injection is introduced, a passive pressure response is observed at the leading edge, producing local vorticity and vortex shedding. The flow mechanism remains the same at both Mach numbers, with a weak sitting vortex near the rear corner. An optimal mass injection pressure ratio is identified.

1. INTRODUCTION

Flow inside a shallow cavity driven by a shear layer is known to be unsteady under a wide range of flow and geometric conditions [1]. Experiments [2, 3] have highlighted the presence of convected vortical structures in the driven shear layer,

0022–460X/99/110023 + 25 $30.00/0

shear layer impingement onto the downstream face and pressure disturbances inside the enclosure, which lead to a self-sustained fluid flow oscillation. This phenomenon is responsible for wall pressure fluctuations, pressure drag increase, and far-field aerodynamic noise radiation.

A substantial amount of research has been directed towards devising means of effective unsteady pressure field control. The objective could be (a) to reduce the pressure drag, (b) to attenuate the pressure fluctuations on aerodynamic surfaces, or (c) to alter the far field noise radiation. Methods have been proposed to modify the flow near the leading edge of the cavity, the shear layer impingement near the trailing edge, and the pressure field inside the cavity. Devices used to modify the pressure field inside the cavity include passive venting of the floor [4] and mass injection near the trailing edge [5]; devices for leading edge flow modifications include spoilers [6, 7], cowls [8], vortex generators [7], and mass injection [9]; Methods for trailing edge shear layer impingement modifications include introducing a ramp [10, 11] and a round-nose [11].

The development/deployment of effective unsteady flow control devices depends on a clear understanding of major flow physics. There are areas of flow physics and their interpretation which deserve further attention. For example, modifying the trailing edge geometry is generally believed to be effective in reducing the pressure fluctuation [10]. Recent model tests [11], however, suggest an enhanced oscillation with certain edge geometries. Devices employed to modify the shear layer generally lead to changes in the dominant mode of oscillation–large vortical structures in the shear layer. This will alter or attenuate narrowband tones observed in the far field. However, as the shear layer is normally turbulent the effects on the likely rise in the broadband noise have not been investigated in depth. Pressure oscillation attenuation mechanisms proposed for some devices such as the leading edge mass injection require further clarification to determine whether the observed reduction in the pressure fluctuation is due to ''active control'' of disturbances in shear layer [9], or in fact an alteration of shear layer impingement. Questions also exist on the effectiveness of a compression ramp and an expansion surface. Would a ''ski-jump'' type of ramp lift the shear layer and modify the downstream reattachment? If so, will the oscillation be attenuated? Will an expansion surface induce a stronger shear layer impingement onto the downstream face, leading to higher pressure fluctuation?

In this study, methods including leading edge compression ramps, expansion surfaces [12], and mass injection are investigated, which follows an earlier study of pressure waves around a cavity [13]. It is hoped that the study will help clarify confusion in the interpretation of model test results. Past experiments suggest that near the leading edge it is possible that unsteady pressure disturbances could selectively excite shear layer instability modes which characterize the time-dependent velocity and vorticity fields. The initial amplitude of such exponentially growing modes provides possibilities for exploring means of reducing or suppressing their onset/growth by altering the flow passing the leading edge. It is also possible that the shear layer reattachment position and characteristics will be altered, leading to changes in the pressure inside the cavity, thus reducing the pressure oscillation. The flows are investigated using

computational fluid dynamics modelling. The calculation solves for the Short-time Reynolds-averaged Navier–Stokes equations (TRANS) with turbulence modelled by a two-equation k–ω model. This follows an earlier study [14] where the numerical model was validated. The authors believe this represents a valid approach as the flow fields concerned are characterized by an unsteady pressure field and are highly susceptible to external disturbances such as a pressure probe in a model test.

2. FLOW CONDITIONS

2.1. BASELINE CASE

The numerical algorithms and model are validated against a baseline model test case: an open two-dimensional cavity flow [2]. The flow is driven by a shear layer from separation of the oncoming boundary layer at the leading edge of the cavity. The length to depth ratio of the cavity is 3 and depth of the cavity is fixed at 15 mm. Freestream Mach numbers are 1·5 and 2·5. The Reynolds number based on the depth of the cavity is $4{\cdot}5 \times 10^5$ at both Mach numbers. In the model tests, a turbulent boundary layer approaches the enclosure upstream edge. At Mach 1·5, the oncoming boundary layer had a thickness δ of $0{\cdot}287\,D$ a displacement thickness δ^* of $0{\cdot}06\,D$, and a momentum thickness θ of $0{\cdot}0273\,D$. At Mach 2·5, the respective values were $0{\cdot}28\,D$, $0{\cdot}0867\,D$, and $0{\cdot}0227\,D$. A schematic of the geometry is shown in Figure 1(a).

2.2. COMPRESSION RAMP AND EXPANSION SURFACE

The approaching surface upstream of the leading edge of the cavity is replaced by compression ramps and expansion surfaces of a fixed length ($1D$). The height of the ramp/surface varies between $0{\cdot}1\,D$, $0{\cdot}2\,D$ and $0{\cdot}4\,D$. The ramps and the surfaces are formed by a circular arc of a constant radius (see Figures 1(b) and (c)).

2.3. MASS INJECTION

In the mass injection test (see Figure 1(d)), the approaching surface upstream of the leading edge of the cavity is replaced by a porous surface extending to $1\,D$ upstream. The porosity factor σ is 0·607 (see section 3). Different back wall pressures are selected. For the Mach 1·5 flow the back wall pressure p_i ranges from $1{\cdot}5\,p_\infty$ to $2{\cdot}5\,p_\infty$; for the Mach 2·5 flow the back wall pressure p_i ranges from $1{\cdot}25\,p_\infty$ to $3{\cdot}0\,p_\infty$.

3. NUMERICAL MODEL

A numerical model of the unsteady flow is obtained through solutions of the discretized short-time averaged Navier–Stokes equations [14] with Wilcox's k–ω turbulence model [15], by which the time dependent predictions are obtained of the large-scale structures characterizing the unsteady flow. The flow field is discretized by using a multi-block structured grid. A second order Roe flux

difference split approximate Riemman solver estimates the inviscid fluxes which are integrated in space with the turbulent fluxes by using a finite volume technique. An explicit multi-step Runge–Kutta scheme with optimized coefficients [16] advances the flow prediction in time. The method is formally second order time and space accurate.

For the majority of the test cases, the computational domain covers an area extending from $x = -3\,D$ to $9\,D$ in the streamwise direction, and from $y = -1\,D$ to $4\,D$ in the transverse direction. The domain above the cavity is covered by 320 by 400 cells and the cavity by 80 by 80 cells. The cell sizes have been found to be adequate for the flow following a cell size test and are therefore retained in this study (for details, see reference [14]). For some cases, the upstream boundary is extended to $x = -6\,D$ as the upstream influence of introducing a ramp and mass injection needs to be taken into account. A fixed turbulent boundary layer is

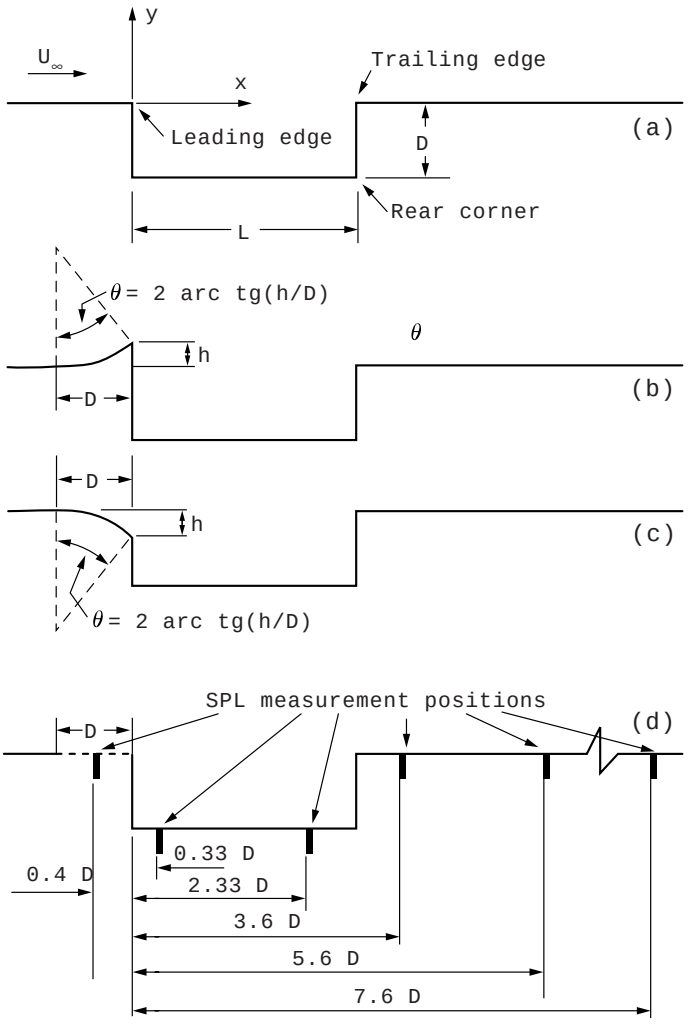

Figure 1. Test geometries: (a) baseline; (b) compression ramp; (c) expansion surface; (d) mass injection.

TABLE 1

Effect of leading edge compression ramp

	Mach 1·5				Mach 2·5			
h/D	Baseline	0·1	0·2	0·4	Baseline	0·1	0·2	0·4
C_d	0·0672	0·1069	0·1511	0·2785	0·0217	0·0345	0·0609	0·1314
St	0·0925	0·0945	0·0952	0·0976	0·0843	0·0839	0·0816	0·0787
$SPL\|_{(-0·4,0)}$	150·3	149·5	163·8	145·2	73·87	113·2	129·5	109·0
$SPL\|_{(0·33,-1)}$	171·1	170·1	168·7	169·9	160·3	157·9	156·1	156·5
$SPL\|_{(2·33,-1)}$	176·0	176·4	176·2	176·3	164·0	162·5	161·6	160·6
$SPL\|_{(3·6,0)}$	168·3	170·3	171·9	174·9	161·3	160·7	158·9	157·7
$SPL\|_{(5·6,0)}$	164·6	165·7	166·8	168·7	155·9	154·9	151·4	149·4
$SPL\|_{(7·6,0)}$	162·8	164·2	166·0	169·8	152·5	151·0	144·9	140·3

defined at the inflow boundary; no-slip conditions are imposed on the solid walls; extrapolated and non-reflecting conditions apply at the outflow ($x = 6\,D$) and upper boundary ($y = 4\,D$), respectively. When the mass injection is considered, a porous surface of constant porosity is introduced. A constant back pressure is maintained below the surface area [17]. According to the linear form of the Darcy pressure–velocity law, this gives

$$v_w = (\sigma/\rho_\infty u_\infty)(p_i - p_w), \tag{1}$$

where σ is the geometric porosity [17] and p_i is the back wall pressure (a list of nomenclature is given in the Appendix).

4. RESULTS AND DISCUSSION

4.1. COMPRESSION RAMP

The changes in the flow field are summarized in Table 1. In terms of Strouhal number (St) and sound pressure level (SPL), the response of the flow to the introduction of a ramp differs at Mach 1·5 and 2·5. At Mach 1·5, there is only a slight rise in St from 0·0925 for the baseline flow to 0·0945 at $h/D = 0{\cdot}1$, 0·0952 at $h/D = 0{\cdot}2$ and 0·0976 at $h/D = 0{\cdot}4$. This compares with a value of 0·093 in the model test. While the SPL on the floor of the cavity experiences negligible changes ($<1{\cdot}4\%$ at $x = 0{\cdot}33\,D$ and $2{\cdot}33\,D$), its value downstream of the cavity rises sharply with h/D, the rise in SPL (compared with the baseline flow) being 2·0 dB at $h/D = 0{\cdot}1$, 3·6 dB at $h/D = 0{\cdot}2$ and 6·6 dB at $h/D = 0{\cdot}4$ being observed at $x = 3{\cdot}6\,D$. A different response with the ramp height is observed at Mach 2·5. Here St drops from 0·0843 for the baseline flow to 0·0839 at $h/D = 0{\cdot}1$, 0·0816 at $h/D = 0{\cdot}2$ and 0·0787 at $h/D = 0{\cdot}4$, which compares with a value of 0·088 from the model test. SPL on the floor as well as downstream of the cavity all experience a reduction in value. The largest reduction occurs near the leading edge, a

reduction of 2·4 dB at $h/D = 0{\cdot}2$, 4·2 dB at $h/D = 0{\cdot}2$ and 3·8 dB at $h/D = 0{\cdot}4$ being observed at $x = 0{\cdot}33\ D$.

A study of the pressure field suggests that the difference in the flow response at the two Mach numbers could not be explained simply by the changes in the mean pressure field. In fact, the influence of the ramp on the mean pressure field is rather similar at the two Mach numbers (see Figure 2). The approaching flow is compressed and a quasi-stationary shock forms in front of the ramp (for a discussion of the pressure waves around a shallow cavity, see references [13, 18]), which is followed by a compression region and then a rapid expansion around the edge of the ramp as the flow is turned around. This leads to a generally low mean pressure environment in the cavity which is indicated by the low mean pressure level on the upstream face of the cavity (see Figure 2). The reduction in the mean pressure level increases with the height of the ramp (h/D). The $h/D = 0{\cdot}4$ ramp produces the lowest mean pressure level at both Mach numbers. This trend continues on the floor of the cavity, while the mean surface pressure rises sharply approaching the rear corner of the cavity due to flow compression as a result of shear layer impingement. The surface mean pressure distribution on the downstream face suggests that the flow is still dominated by a large sitting vortex

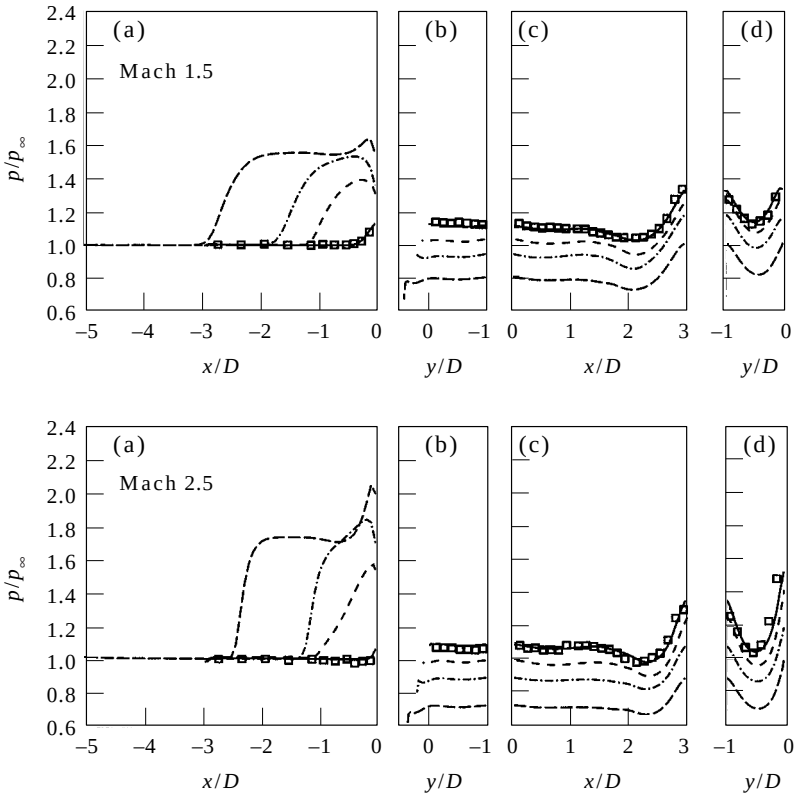

Figure 2. Surface mean pressure with compression ramps: (a) approaching surface; (b) upstream face; (c) floor; (d) downstream face. □, Test; —, baseline; - - - , $h/D = 0{\cdot}1$; - · - · - , $h/D = 0{\cdot}2$; – – – , $h/D = 0{\cdot}4$.

in the region near the rear corner [2]. In presenting the results, we define a mean pressure drag coefficient, C_d, taking into account the pressure on the upstream face, the downstream face, the ramp and the expansion surface. Thus, for the baseline geometry

$$C_d = \int_{-D}^{0} \frac{p_{down} - p_{up}}{q} \, dy; \tag{2}$$

for the expansion surface geometry,

$$C_d = \int_{-D}^{0} \frac{p_{down}}{q} \, dy - \int_{-D}^{-h} \frac{p_{up}}{q} \, dy - \int_{-h}^{0} \frac{p_{exp}}{q} \, dy; \tag{3}$$

for the ramp geometry,

$$C_d = \int_{-D}^{0} \frac{p_{down}}{q} \, dy - \int_{-D}^{h} \frac{p_{up}}{q} \, dy + \int_{0}^{h} \frac{p_{ramp}}{q} \, dy. \tag{4}$$

It can be seen from Table 1 that the mean pressure drag coefficient is increased sharply with h/D. At Mach 1·5, C_d rises to 1·59 times that of the baseline flow at $h/D = 0{\cdot}1$, 2·25 times at $h/D = 0{\cdot}2$, and 4·14 times at $h/D = 0{\cdot}4$. At Mach 2·5, the corresponding values are 1·59, 2·81 and 6·06. This is mainly due to the presence of the ramp. In fact, the characteristics of the surface mean pressure in the cavity are quite similar.

Changes in the unsteady flow field (see Table 1 and Figure 3) involve variations in both frequency and magnitude. These behave differently at Mach 1·5 and 2·5, suggesting a difference in the physics. In Figure 3 only the baseline case and $h/D = 0{\cdot}2$ case are presented. The characteristics of the $h/D = 0{\cdot}1$ and 0·4 flows are rather similar to those at $h/D = 0{\cdot}2$ and are therefore not presented. To understand the observed flow features, a clear understanding of the basic flow physics is necessary. We believe that one important aspect of the flow is a coupled motion of the shear layer [13], the results of which can be seen in the velocity vectors in Figures 4 and 5, where a sequence of the flow motion is presented and the corresponding surface pressure variations are given in Figure 6. In the transverse direction, the shear layer experiences a flapping motion due to the shear layer instability. In the streamwise direction, there is a vortex convection due to the non-linear propagation effects leading to significant wave steepening with convection. These two motions are strongly coupled. At Mach 1·5, the instability of the shear layer is rather strong and the non-linear propagation effects are such that the wave steepening with convection produces large convective vortices (Figure 4), leading to the transient pressure in the cavity (Figure 6). The flapping motion of the shear layer is thus quite pronounced and causes the large vortex near the rear corner to experience large motion in the transverse direction. As a result of this coupled motion, although the unsteady mode is in the longitudinal direction, the induced pressure fluctuation is characterized by the flapping motion of the shear layer near the trailing edge. The (vertical) flapping motion of the shear

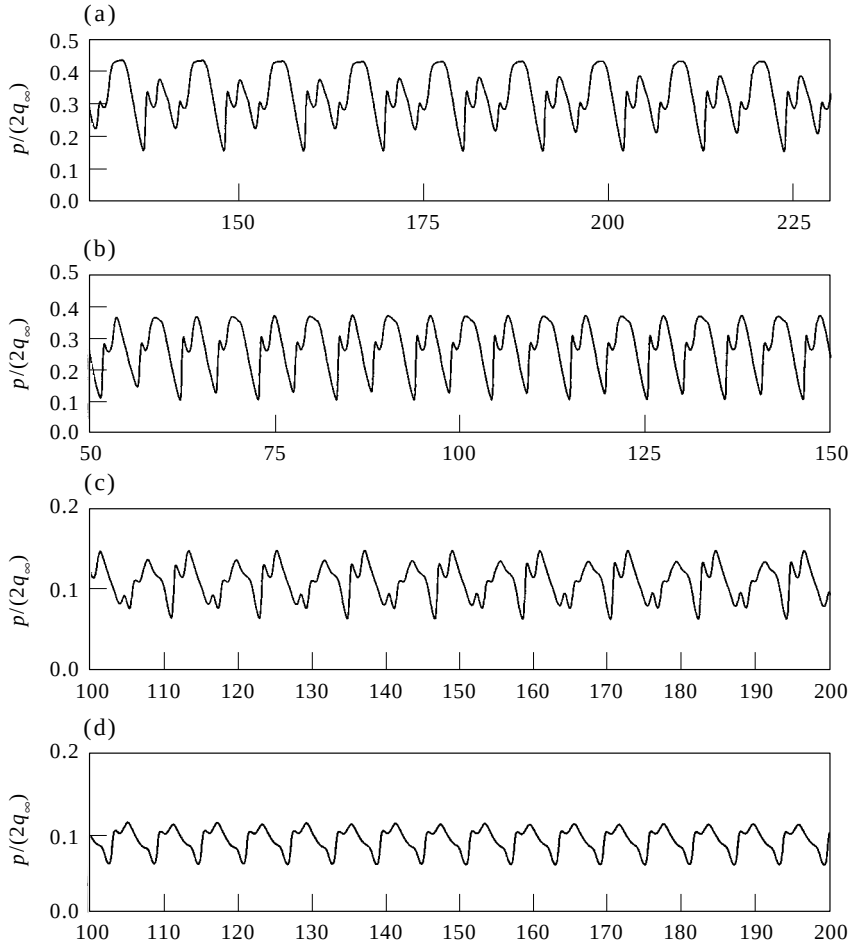

Figure 3. Surface pressure with compression ramps at $x/D = 2{\cdot}33$: (a) baseline at Mach 1·5; (b) $h/D = 0{\cdot}2$ at Mach 1·5; (c) baseline at Mach 2·5; (d) $h/D = 0{\cdot}2$ at Mach 2·5.

layer near the trailing edge is geometrically limited to the depth of of the cavity. The length scale of this flapping motion is therefore primarily determined by a flow-independent geometric restriction and so remains constant at value near 1 D. Consequently the observed St value does not change significantly with h/D. As the trailing edge is now lower than the leading edge with a ramp, the strongly amplified disturbances/vortex structures are allowed to be convected downstream of trailing edge (see Table 1).

At Mach 2·5, the instability of the shear layer is weak (the limiting Mach number for a vortex sheet is $2\sqrt{2}$ above which the vortex sheet is stable [19]). The non-linear effect is times rather weak, producing small vortices convecting in the longitudinal direction. The large vortex near the trailing edge (see Figure 5) experiences a relatively smaller motion in the transverse direction than that of the Mach 1·5 flow and the unsteady motion/pressure field is then dominated by the convected disturbances/vortices in the longitudinal direction. As a result of this, St drops with the ramp height h/D as the distance between the edge of the ramp

and the trailing edge increases with h/D. The level of oscillation in terms of *SPL* is lower than that of the baseline flow at Mach 2·5.

4.2. EXPANSION SURFACE

When a leading edge expansion surface is introduced, the pressure field in the cavity is affected and the presence of the expansion surface acts as a limiting factor in defining the pressure level in the cavity. This feature can be observed in Figure 7 where the surface mean pressure is given. There are two important features of the mean flow: (i) unlike the ramp case, the mean pressures on the upstream face

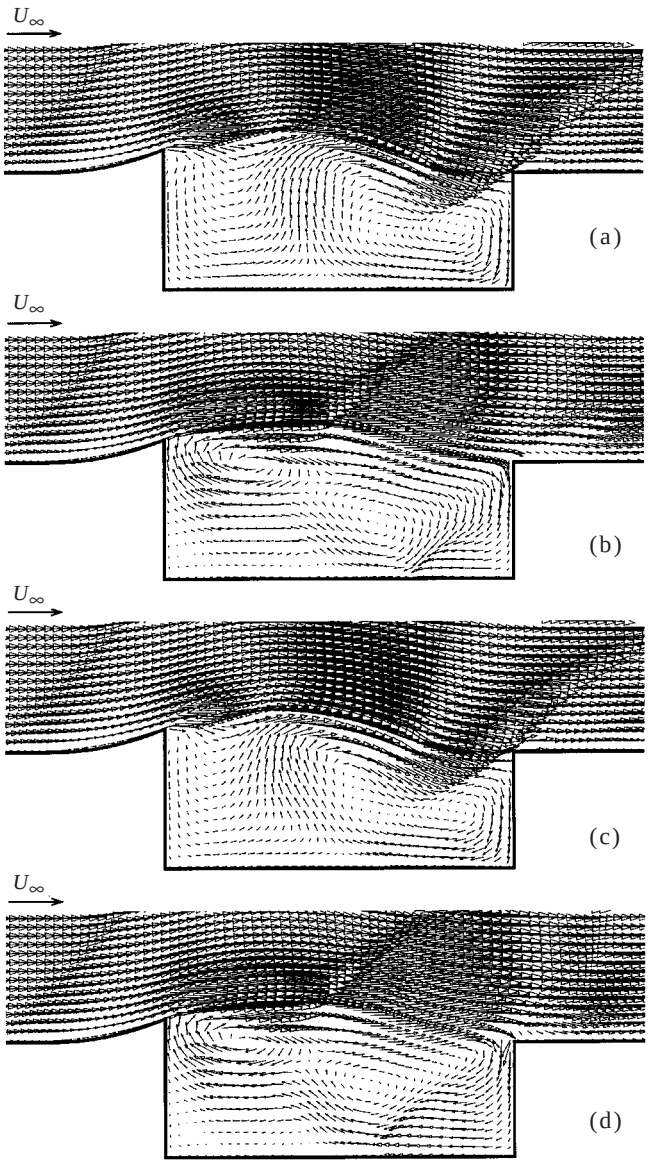

Figure 4. Velocity vectors with a $h/D = 0{\cdot}2$ compression ramp at Mach 1·5 over one period T: (a) $t = 0$; (b) $t = 0{\cdot}25\ T$; (c) $t = 0{\cdot}5\ T$; (d) $t = 0{\cdot}75\ T$.

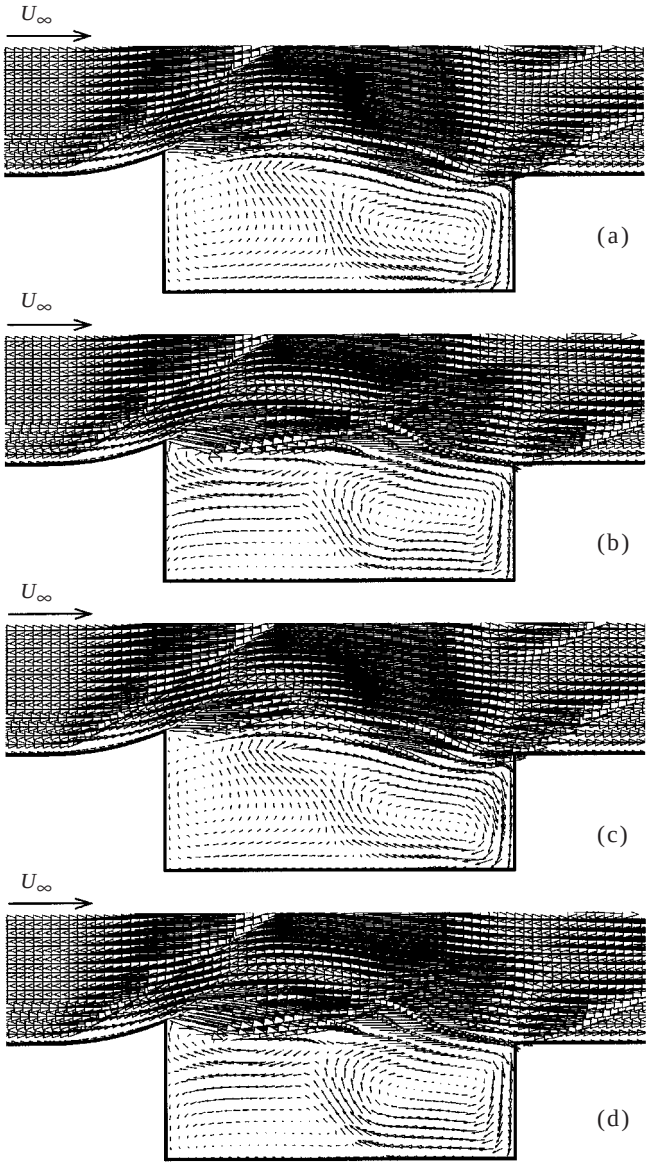

Figure 5. Velocity vectors with a $h/D = 0{\cdot}2$ compression ramp at Mach 2·5 over one period T: (a) $t = 0$; (b) $t = 0{\cdot}25\ T$; (c) $t = 0{\cdot}5\ T$; (d) $t = 0{\cdot}75\ T$.

(see Figure 7(b)) are nearly the same at the three heights; (ii) the sitting vortex near the rear corner (see Figure 7(d)) is weaker than that of the baseline case, suggesting a weak shear layer impingement. The second feature is rather surprising as it is expected the expansion surface would lead to a stronger shear layer impingement which will then produce high surface mean pressure on the downstream trailing edge, and more importantly stronger pressure feedback and fluctuation in the cavity. The fact that a weaker vortex is produced suggests that the separated shear layer from the leading edge possesses different features from that of the baseline

case. When the oncoming flow approaches the leading edge, the expansion surface allows the flow to accelerate along the surface, hence the reduction in the surface mean pressure (see Figure 7(a)) and associated expansion pressure waves (see density contours in late figures). However, this process is terminated on the surface by an oblique shock wave. The leading edge oblique shock wave is rather similar to the type 2 wave described in reference [18] and type 1 wave of reference [13]. The appearance of the wave depends on the height of the expansion surface. The higher the surface the earlier the appearance of the terminating shock wave, and the stronger the wave. The surface mean pressure is at its lowest at $h/D = 0{\cdot}4$ under the present flow conditions. Downstream of the oblique wave the pressure recovers. The extent of the pressure recovery, though, depends on the flow following the shock wave. For the $h/D = 0{\cdot}1$ and $0{\cdot}2$ cases, the pressure recovery processes are rather similar, leading to a surface mean pressure level close to that of the baseline case at $x = 0$ (see Figure 7(a)). At $h/D = 0{\cdot}4$, the recovery process

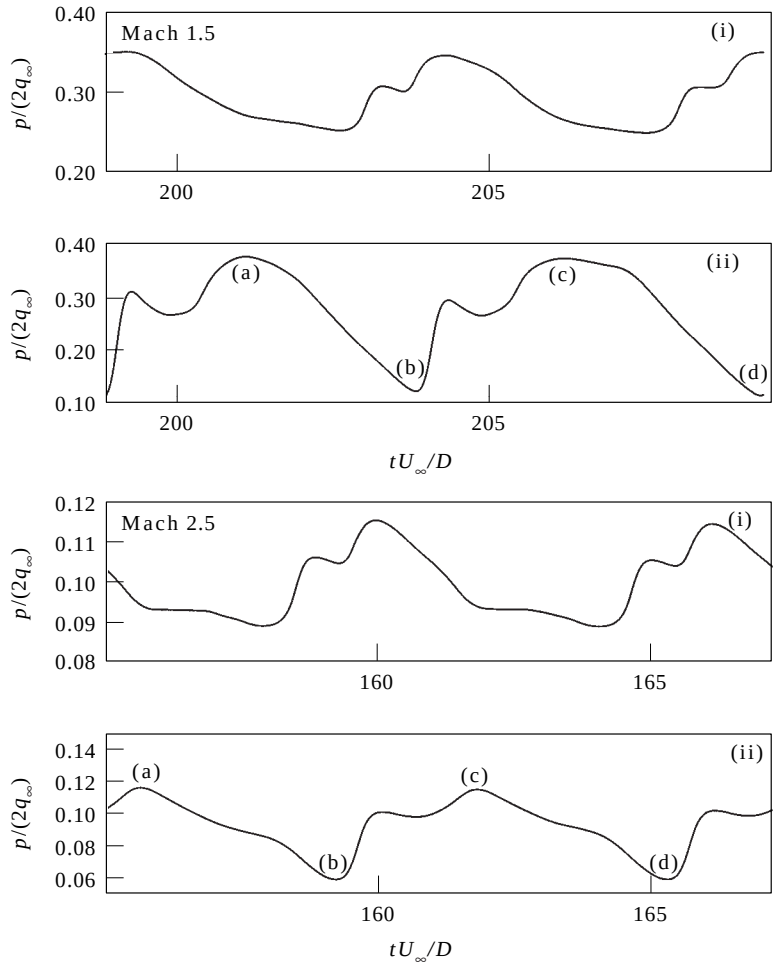

Figure 6. Surface pressure over one period with a $h/D = 0{\cdot}2$ compression ramp: (i) $x/D = 0{\cdot}33$; (ii) $x/D = 2{\cdot}33$.

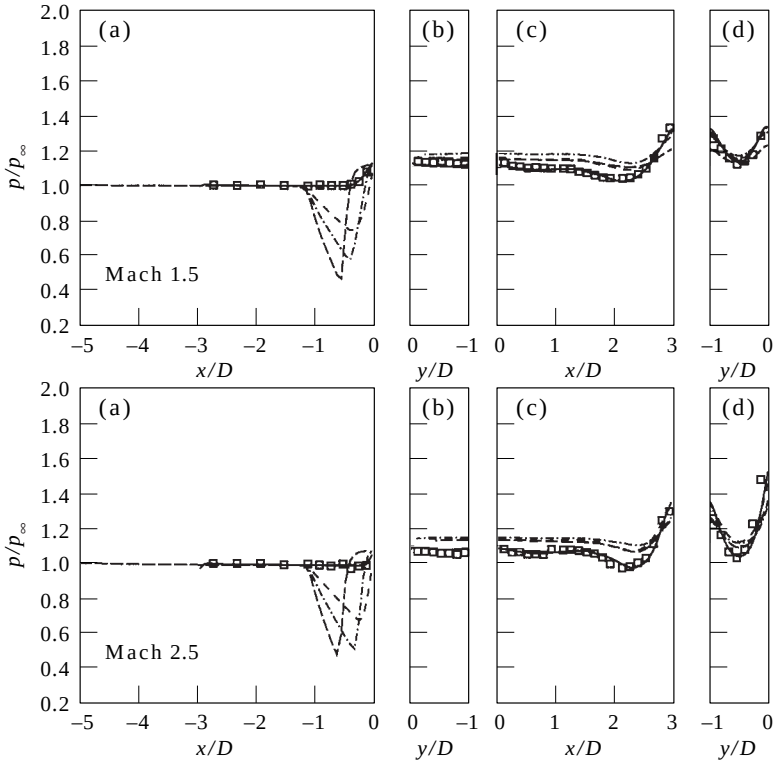

Figure 7. Surface mean pressure with expansion surfaces: (a) approaching surface; (b) upstream face; (c) floor; (d) downstream face. □, Model test; —, baseline; - - - , $h/D = 0{\cdot}1$; - · - · - , $h/D = 0{\cdot}2$; – – – , $h/D = 0{\cdot}4$.

is slightly different at both Mach numbers. There is an area of relatively high surface pressure approaching $x = 0$ (leading edge) at both Mach 1·5 and 2·5. In fact, the surface mean pressures at Mach 1·5 and 2·5 possess the same characteristics. It will be shown (later with the velocity vectors) that a shock induced flow separation occurs at $h/D = 0{\cdot}4$ at both Mach numbers. The resulting recircuiting flow from the flow separation is associated with nearly stable flow environment at Mach 1·5 and stable flow at Mach 2·5. From Table 2, it can be seen that the pressure drag coefficient is increased with the leading edge expansion surfaces. The increase though is not as big as that with a compression ramp.

The accelerated flow along the expansion surface alters the stability characteristics of the shear layer from the flow separation at the leading edge at $h/D = 0{\cdot}1$ and 0·2 at both Mach numbers. The pressure fluctuations are reduced significantly by the introduction of the surfaces (see Figures 8 and 9, and Table 2). In Figure 8, the pressure fluctuations at $h/D = 0{\cdot}2$ show a big reduction compared with that of a baseline flow (see Figure 3). At $h/D = 0{\cdot}4$, the flow is nearly stable and the oscillation is very weak, *SPL* being about 35 dB lower than that for the baseline flow. At Mach 2·5 (see Figure 9), the flow is completely stable after an initial period of the starting process of the numerical computation [14]. The characteristics of the flows at Mach 1·5 and 2·5 are the same. The reduction

TABLE 2

Effect of leading edge expansion surface

	Mach 1·5				Mach 2·5			
h/D	Baseline	0·1	0·2	0·4	Baseline	0·1	0·2	0·4
C_d	0·0672	0·0645	0·0786	0·0787	0·0217	0·0267	0·0245	0·0306
St	0·0925	0·0893	0·0859	0·0823	0·0843	0·0804	0·0786	n/a
$SPL\|_{(-0·4,0)}$	150·3	154·0	162·0	142·0	73·87	105·7	127·3	n/a
$SPL\|_{(0·33,-1)}$	171·1	169·8	169·5	136·0	160·3	158·1	151·1	n/a
$SPL\|_{(2·33,-1)}$	176·0	174·2	171·3	139·0	164·0	164·3	152·9	n/a
$SPL\|_{(3·6,0)}$	168·3	166·0	161·8	131·0	161·3	158·8	147·2	n/a
$SPL\|_{(5·6,0)}$	164·6	162·6	159·3	126·4	155·9	152·9	139·4	n/a
$SPL\|_{(7·6,0)}$	162·8	160·2	157·4	125·5	152·5	148·8	132·7	n/a

in the pressure oscillation occurs not only in the cavity but downstream after the reattachment of the shear layer (see Table 2). A typical example is Mach 2·5 flow at $h/D = 0·2$, where the SPL experiences a reduction of around 10 dB in the cavity and a bigger reduction downstream.

The difference between the stable flow and the unsteady flow is shown in Figures 10 and 11. In Figure 10, the attenuated and nearly stable flow at Mach 1·5 is shown with the velocity vectors and the density contours. Figure 11 gives examples of the

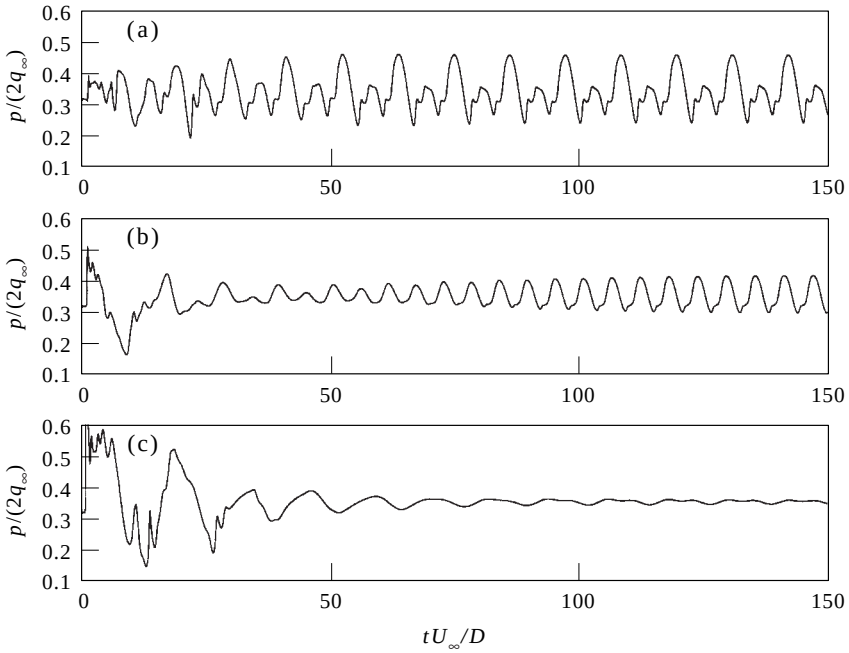

Figure 8. Surface pressure with expansion surfaces at $x/D = 2·33$ and Mach 1·5. h/D values: (a) 0·1; (b) 0·2; (c) 0·4.

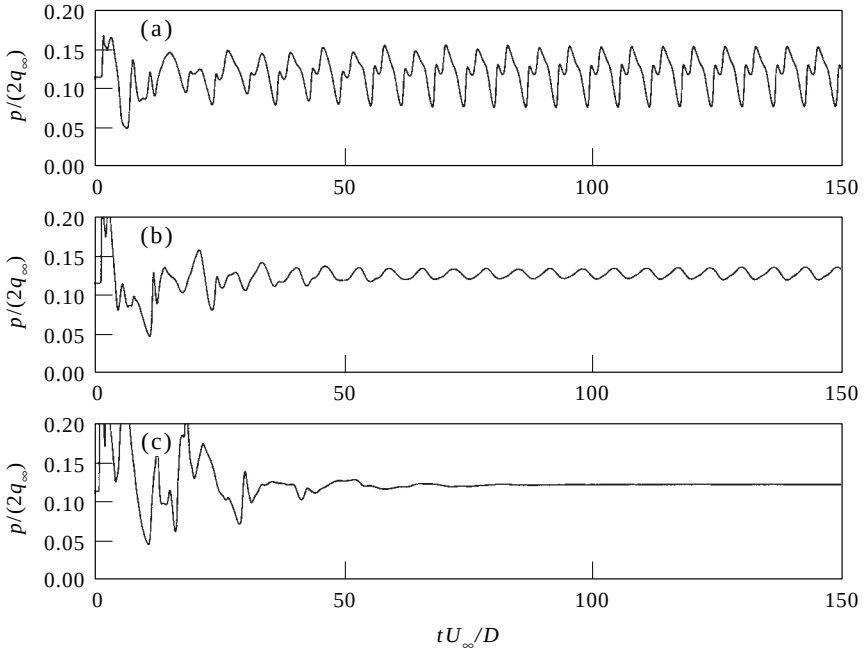

Figure 9. Surface pressure with expansion surfaces at $x/D = 2{\cdot}33$ and Mach 2·5. h/D values; (a) 0·1; (b) 0·2; (c) 0·4.

unsteady flow at Mach 1·5 and $h/D = 0{\cdot}2$. As the unsteady flow physics are rather similar with an expansion surface at Mach 1·5 and 2·5, only the Mach 1·5 results are discussed here. At $h/D = 0{\cdot}1$ and 0·2, the observed flow physics such as the sitting vortex and the pressure waves are similar. Therefore, only $h/D = 0{\cdot}2$ results are given in Figure 11, In Figure 11, the flow on the expansion surface is shown to stay attached during the whole period of flow oscillation. In Figure 11(a), the flow is associated with local low pressure near the leading edge and a downward deflection of the shear layer into the cavity. The position of the large sitting vortex near the trailing edge suggests a mass ejection process near the trailing edge [14]. In Figure 11(b), the upward deflection of the shear layer at the leading edge is associated with local high pressure and the creation of a convecting vortex near (but not at) the leading edge. The sitting vortex near the rear corner suggests a mass entrainment process at the trailing edge [14].

In Figure 10, the density contours show the wave patterns above the cavity, in particular the expansion–shock wave system on the expansion surface (see Figure 10(b)). In viewing the velocity vectors at $h/D = 0{\cdot}4$ where the flow is nearly stable, it is interesting to note the induced flow separation on the expansion surface following the limiting oblique shock wave. The reversed flow indicates an induced separation and the resulting vortex/vorticity distribution is also clear. This vortex/vorticity distribution differs from those observed in Figures 4 and 5, and Figure 11. When the flow is unstable (e.g., with a compression ramp), the shear layer from the leading edge flow separation is unstable. The amplification of the instability waves leads to significant wave steepening and convecting vortices.

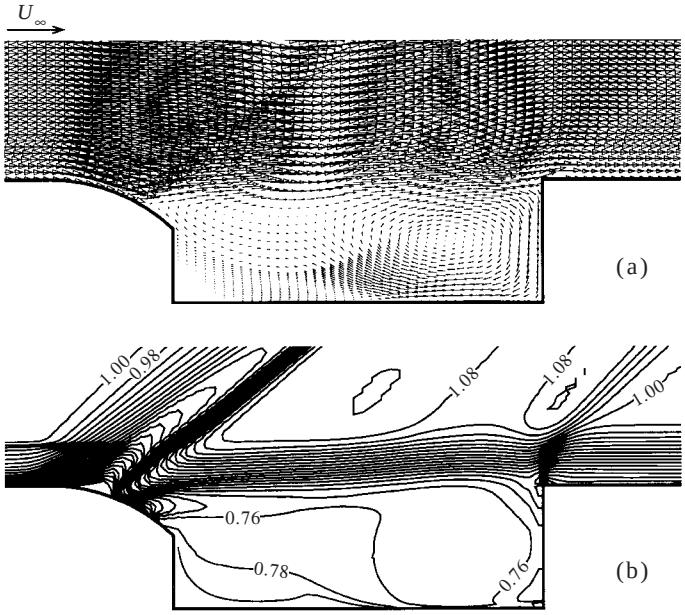

Figure 10. Steady flow at Mach 1·5 with a $h/D = 0{\cdot}4$ expansion surface: (a) velocity vectors; (b) ρ/ρ_∞ contours.

These vortices are not produced at the leading edge but some distance downstream. In the current flow at $h/D = 0{\cdot}4$, the vorticity produced by the flow separation on the expansion surface is located on the surface and is not convected

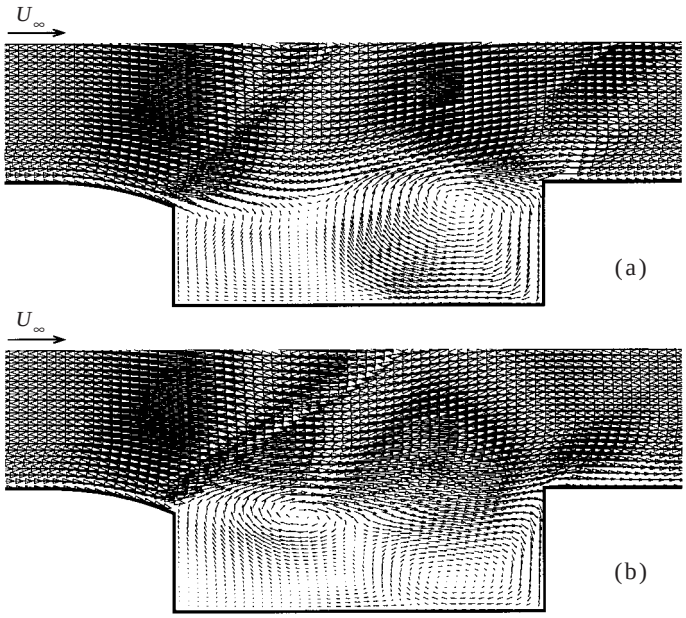

Figure 11. Unsteady flow at Mach 1·5 with a $h/D = 0{\cdot}2$ expansion surface: (a) downward deflection of shear layer at the leading edge; (b) upward deflection.

TABLE 3

Mach 1·5 *flow with leading edge mass injection*

p_i/p_∞	Baseline	1·5	2·00	2·25	2·50
$\langle \rho v \rangle$	n/a	0·0293	0·1018	0·1582	0·2058
C_d	0·0672	0·0388	0·0150	0·0139	0·0147
St	0·0925	0·0892	0·0805	0·0730	0·0756
$SPL\|_{(-0·4,0)}$	150·3	155·4	153·3	154·7	155·5
$SPL\|_{(0·33,-1)}$	171·1	168·4	160·8	160·0	162·3
$SPL\|_{(2·33,-1)}$	176·0	173·3	165·0	163·6	165·7
$SPL\|_{(3·6,0)}$	168·3	168·1	159·1	159·1	161·0
$SPL\|_{(5·6,0)}$	164·6	164·0	150·6	152·4	155·4
$SPL\|_{(7·6,0)}$	162·8	163·0	144·8	151·9	154·1

and no convected vortex forms. This changes the shear layer stability characteristics and leads to a stable flow. The dominant feature of the flow at $h/D = 0·4$ is thus the sitting vortex near the trailing edge/downstream face. We have earlier noticed from the surface mean pressure (see Figure 7(d)) that the sitting vortex is weaker than that of the baseline flow. It should be mentioned here that the complex flow physics described above, in particular the shock/boundary layer interaction on the expansion surface, is simulated with a two-equation k–ω turbulence model. Questions remain as to the applicability of the turbulence model to this flow, which could be answered with a model experiment.

4.3. MASS INJECTION

For the mass injection study, the calculated values of Strouhal number, sound pressure level and mean pressure drag coefficient are given at different pressure ratios and mean mass flow rates in Tables 3 and 4. The mass injection generally introduces a significant drop in the sound pressure level. At Mach 1·5, the largest

TABLE 4

Mach 2·5 *flow with leading edge mass injection*

p_i/p_∞	Baseline	1·25	1·50	2·00	2·25	2·50	2·75	3·00
$\langle \rho v \rangle$	n/a	n/a	0·0085	0·0223	0·0319	0·440	0·0568	0·0587
C_d	0·0217	0·0193	0·0146	0·0052	0·0044	0·0047	0·0066	0·0065
St	0·0843	0·0829	0·0813	0·0758	0·0724	0·0691	0·0657	0·0263
$SPL\|_{(-0·4,0)}$	73·88	108·9	134·6	142·1	140·4	141·1	143·0	145·1
$SPL\|_{(0·33,-1)}$	160·3	158·6	152·1	152·3	149·2	148·3	148·7	149·9
$SPL\|_{(2·33,-1)}$	164·0	163·2	162·6	158·3	155·5	154·5	154·8	156·0
$SPL\|_{(3·6,0)}$	161·3	160·7	159·8	154·1	148·9	144·5	143·7	146·5
$SPL\|_{(5·6,0)}$	155·9	155·1	153·7	145·1	141·2	139·4	138·9	142·4
$SPL\|_{(7·6,0)}$	152·5	151·6	149·9	140·8	135·0	139·4	141·3	141·8

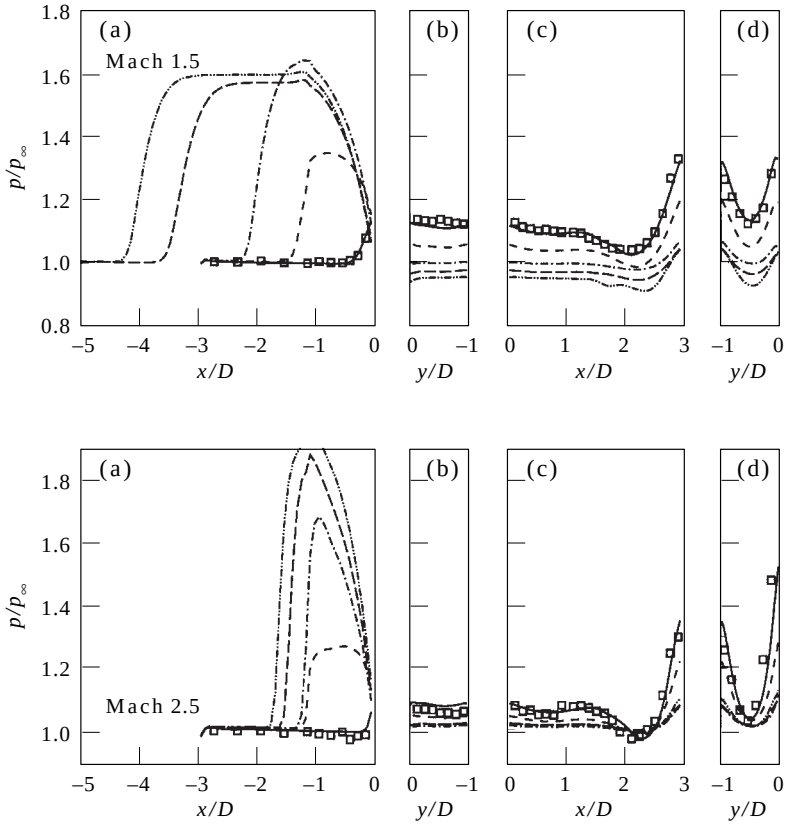

Figure 12. Surface mean pressure with mass injection: (a) approaching surface; (b) upstream face; (c) floor; (d) downstream face. □, Test; —, baseline; - - - -, $p_i/p_\infty = 1{\cdot}5$; - · - · - ·, $p_i/p_\infty = 2{\cdot}0$; – – –, $p_i/p_\infty = 2{\cdot}25$; – · · – · · –, $p_i/p_\infty = 2{\cdot}5$.

reduction in the cavity is observed at $p_i/p_\infty = 2{\cdot}25$, being 11·1 dB at $x = 0{\cdot}33\ D$ and 12·4 dB at $x = 2{\cdot}33\ D$. Increasing p_i/p_∞ above 2·25 will not produce a further reduction in *SPL*. At Mach 2·5, the largest reduction in *SPL* on the floor is observed at $p_i/p_\infty = 2{\cdot}5$, where a drop of 12 dB is observed at $x = 0{\cdot}33\ D$. Again, a further increase in the mass flow rate of p_i/p_∞ will not lead to a further drop in *SPL*. In Tables 3 and 4, the mean pressure drag coefficient is seen to experience a significant drop in value with p_i/p_∞. A nearly five-fold reduction is observed at both Mach numbers.

The mean surface pressure distribution is given in Figure 12. Unlike the compression ramp test cases, the mean pressure distribution does exhibit some different features from the baseline cases, notably on the downstream face. The mean pressure distribution on the downstream face, however, does point to the existence of a large sitting vortex and the surface mean pressure distribution is that of a typical vortex flow induced one. With the mass injection, it can be seen that the difference in the mean pressure is reduced, suggesting a weakened sitting vortex near the rear corner. On the mean flow field, there is again a quasi-stationary oblique shock in front of the mass injection region, followed by a compression region and then an expansion region near the leading edge. As a result, the mean

pressure field in the cavity is generally lower than the corresponding one for the baseline flow. An interesting feature of the flow is that a high p_i/p_∞ or mean $\langle \rho v \rangle$ does not necessarily lead to a low pressure drag coefficient. The lowest pressure drag coefficient is observed at $p_i/p_\infty = 2{\cdot}5$ at both Mach numbers. At Mach 2·5, the mean pressure distribution shows little change between $p_i/p_\infty = 2{\cdot}0$ and 3·0, despite the increase in the mean mass flow rate $\overline{\langle \rho v \rangle}$. In explaining the behaviors of the mean pressure drag coefficient and *SPL* with the mass flow rate, it is interesting to note the rise in the surface mean pressure upstream of the cavity (see Figure 12). The rise in the mean pressure above $p_i/p_\infty = 2{\cdot}0$ is quite marginal and, in the case of the Mach 1·5 flow, small. It follows that the expansion of the flow around the leading edge remains similar for further increase of p_i/p_∞. An optimal pressure rate for both mean form drag coefficient and *SPL* reduction could then be possible, and indeed is identified in the study at 2·5 based on the mean pressure drag coefficient.

The reduction in *SPL* can be seen clearly in Figures 13 and 14, where the unsteady surface pressure variations are presented. At both Mach numbers, the Strouhal number is reduced substantially with the mass injection. At Mach 1·5, *St* drops from 0·0925 for the baseline flow to 0·073 at $p_i/p_\infty = 2{\cdot}25$. At Mach 2·5, *St* drops from 0·843 for the baseline flow to 0·0724 at $p_i/p_\infty = 2{\cdot}25$. The reduction

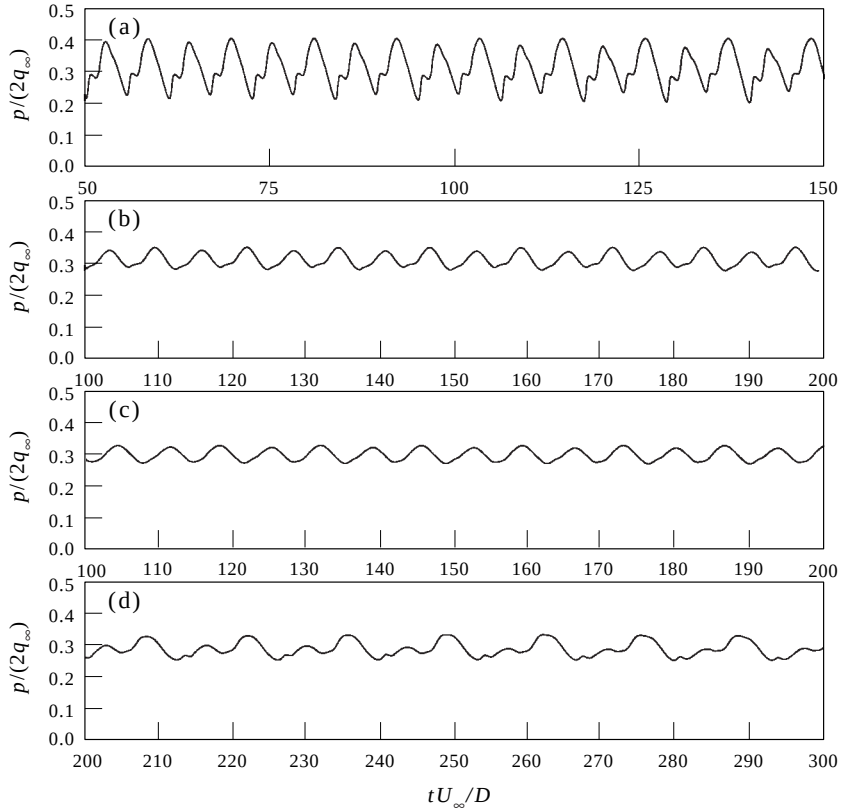

Figure 13. Surface pressure injection at $x/D = 2{\cdot}33$ and Mach 1·5. p_i/p_∞ values: (a) 1·5; (b) 2·0; (c) 2·25; (d) 2·5.

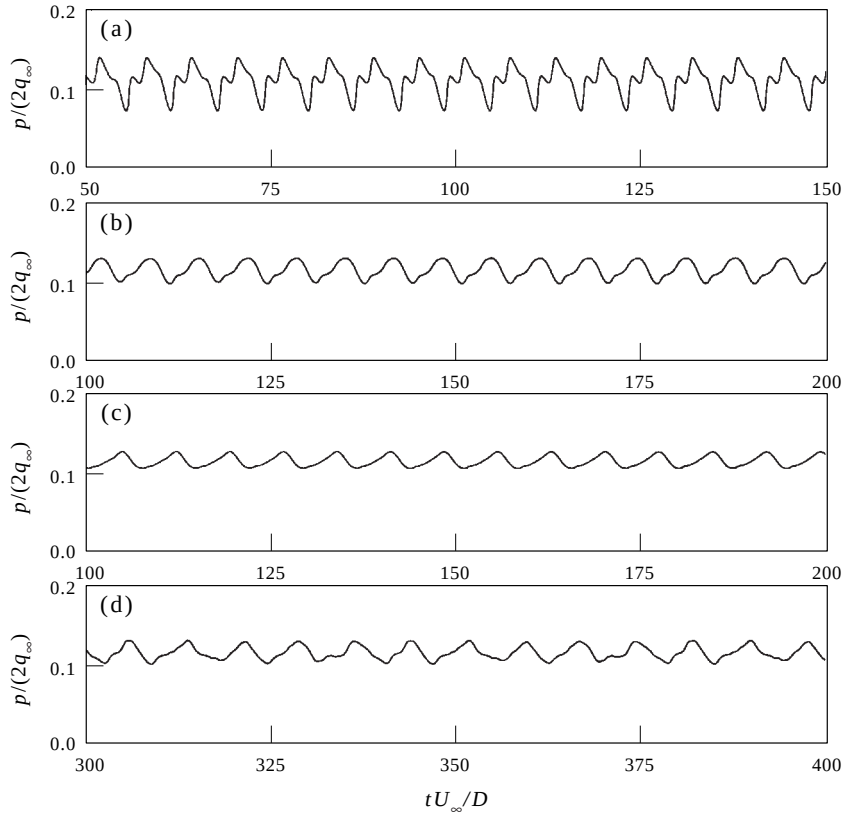

Figure 14. Surface pressure with mass injection at $x/D = 2{\cdot}33$ and Mach 2·5. p_i/p_∞ values: (a) 1·5; (b) 2·0; (c) 2·5; (d) 3·0.

in the Strouhal number at both Mach numbers can be explained by the low convection speed of the vortices in the shear layer following the mass injection. In Figures 15 and 16, velocity vectors at four consecutive times in one oscillation period are given for a typical pressure ratio. The monitored mass flow rate and surface pressures upstream and on the floor of the cavity are presented for the same period in Figures 17 and 18. It can be seen that $\langle \rho v \rangle$ responds passively to the unsteady pressure at the leading edge. A high local pressure leads to a low mass flow rate, while a high mass flow rate corresponds to a low local pressure. As a result of the local passive pressure response, a local transient velocity/vorticity field near the leading edge is generated. A vortex is produced immediately after the leading edge but its strength is rather weak in comparison with that observed in the ramp test cases under similar flow conditions (see Figure 4). We have seen that due to this particular physics the flow oscillation mechanism remains the same at both Mach numbers (see Figures 13 and 14). In Figures 15 and 16, the sitting vortex near the trailing edge is weak in comparison with that in the baseline cases and the ramp cases. Although not presented in the paper, the pressure wave patterns at Mach 1·5 and 2·5 are rather similar to those reported by Zhang *et al*. [13]. Apart from the unsteady waves around the trailing edge due to the shear layer

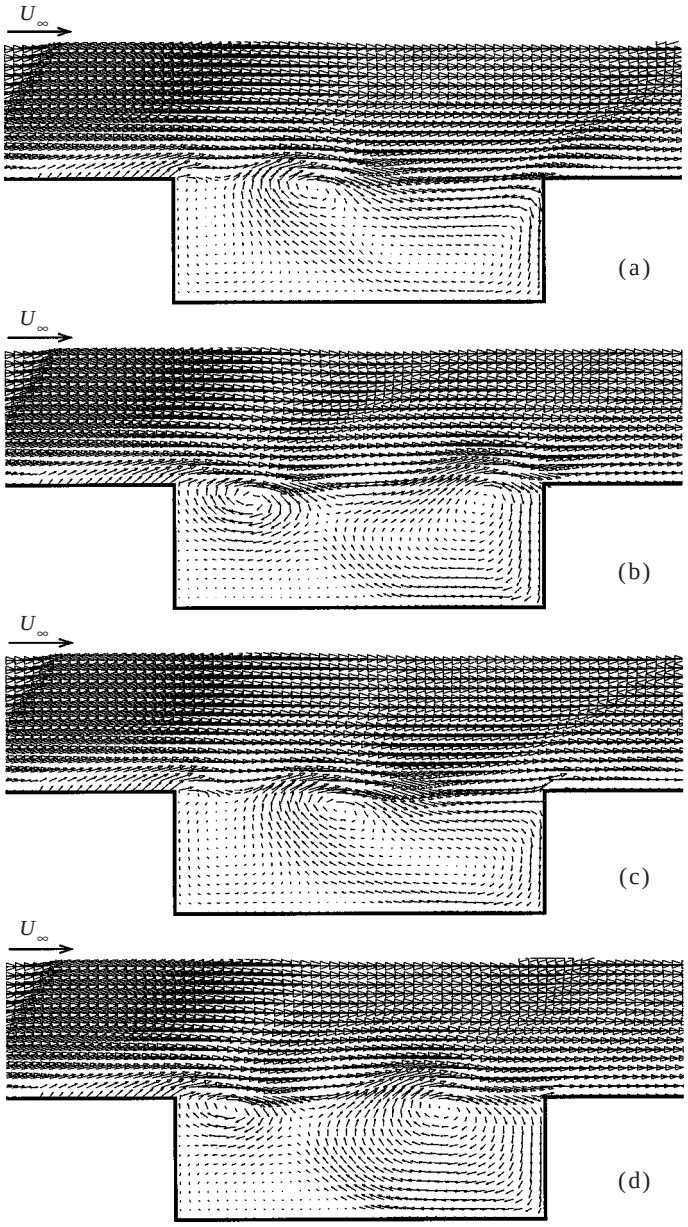

Figure 15. Velocity vectors at Mach 1·5 and $p_i/p_\infty = 2{\cdot}0$ over one period T: (a) $t = 0$; (b) $t = 0{\cdot}25\ T$; (c) $t = 0{\cdot}5\ T$; (d) $t = 0{\cdot}75\ T$.

flapping, the convective vortices also induce an associated wave which is convected downstream.

5. CONCLUDING REMARKS

The effects of leading edge compression ramps, expansion surfaces and mass injection on supersonic shallow cavity flow oscillations are investigated, through

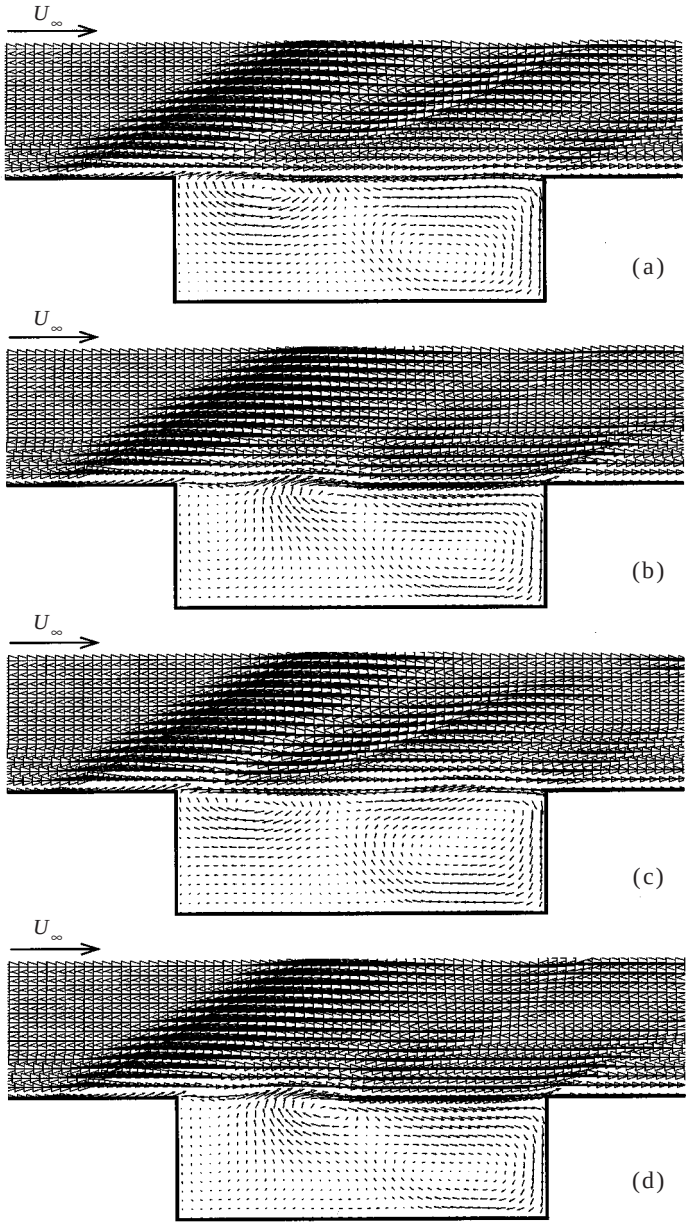

Figure 16. Velocity vectors at Mach 2·5 and $p_i/p_\infty = 2{\cdot}0$ over one period T: (a) $t = 0$; (b) $t = 0{\cdot}25\ T$; (c) $t = 0{\cdot}5\ T$; (d) $t = 0{\cdot}75\ T$.

solutions of Short-time Reynolds-Averaged Navier–Stokes equations with the effect of turbulence modelled by a two-equation k–ω model. This study has provided insight into major flow physics and clarified confusion in the interpretation of the effectiveness of different means for the unsteady flow control.

The findings are as follows.

1. The shear layer driven oscillation is characterized by a coupled motion of shear layer flapping in the transverse direction due to the shear layer instability,

and vortex convection in the streamwise direction due to the non-linear propagation effects leading to significant wave steepening with convection. This mechanism explains different responses to the introduction of a leading edge compression ramp at Mach 1·5 and 2·5.

2. At Mach 1·5, the shear layer is dominated by large non-linear roll-ups of convective vortices which lead to a strong flapping motion of shear layer near the trailing edge. The limiting length scale of the oscillation is the depth of the cavity. The Strouhal number of the oscillation and *SPL* experience small changes with h/D. With the introduction of a ramp, the large vortical structures are convected downstream beyond the trailing edge of the cavity and enhanced pressure fluctuations are observed downstream of the cavity as compared with the baseline flow.

3. At Mach 2·5, a reduction in both the Strouhal number and *SPL* in and around the cavity is observed. The non-linear effect is small at this Mach number and the oscillation is in the longitudinal direction, with smaller shear layer flapping in the transverse direction near the trailing edge. The increased length between the edge of the ramp and the trailing edge thus leads to the reduction in St.

4. When an expansion surface is introduced, an expansion wave is formed on the surface which is terminated by an oblique shock. At a high surface height of $h/D = 0{\cdot}4$, a shock induced flow separation occurs on the surface, inducing a sitting vortex or vorticity distribution which is not convected downstream. A nearly stable flow is established at Mach 1·5 and stable flow at Mach 2·5.

5. When mass injection is introduced on the surface upstream of the leading edge, a passive pressure response is generated which modulates the mass flow rate.

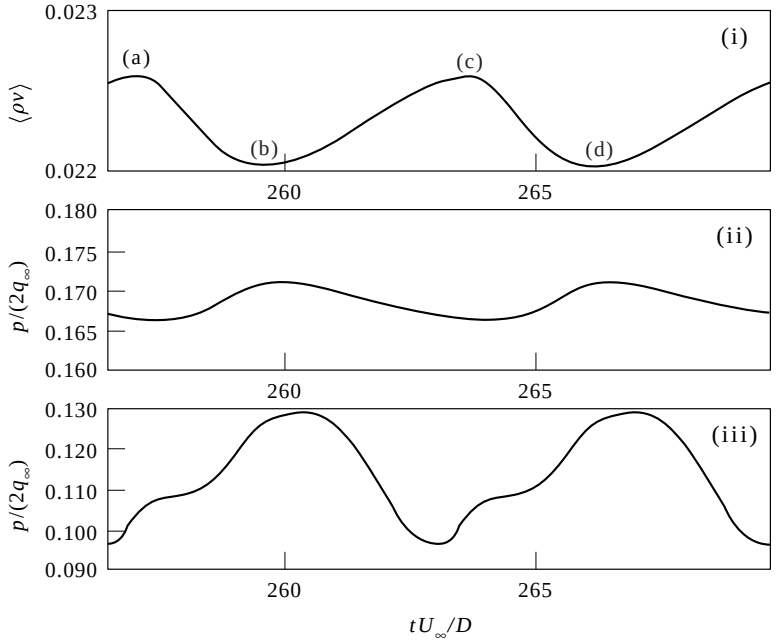

Figure 17. Variation of mass flow rate and surface pressure over one period at Mach 1·5 and $p_i/p_\infty = 2{\cdot}0$: (i) $\langle \rho v \rangle$; (ii) $x/D = -0{\cdot}4$; (iii) $x/D = 2{\cdot}33$.

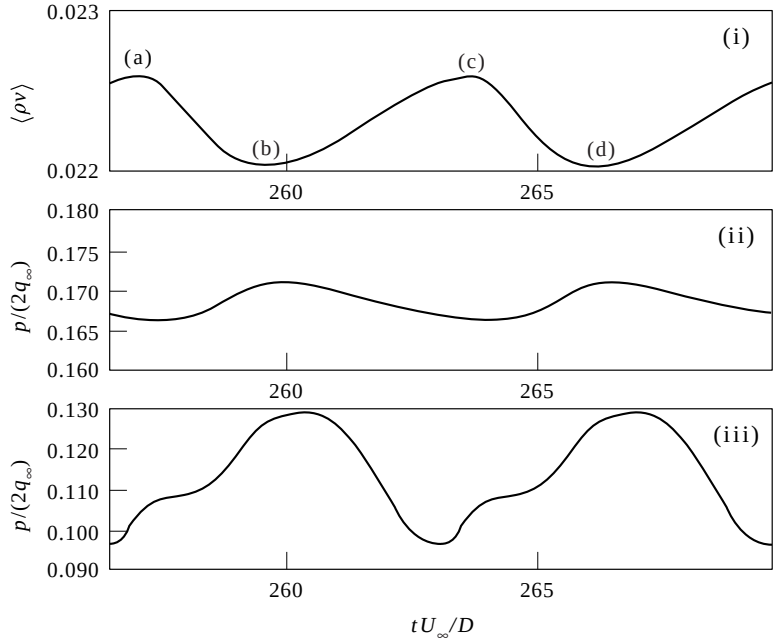

Figure 18. Variation of mass flow rate and surface pressure over one period at Mach 2·5 and $p_i/p_\infty = 2{\cdot}0$: (i) $\langle \rho v \rangle$; (ii) $x/D = -0{\cdot}4$; (iii) $x/D = 2{\cdot}33$.

Local vorticity is produced immediately after the leading edge, leading to vortex convection in the longitudinal direction. The flow physics remains the same at both Mach numbers. Rsults suggest a reduction in *St*, *SPL*, and mean pressure drag coefficient. The reduction in *SPL* could be as much as 10 dB.

6. The biggest reduction in *SPL* and mean pressure drag coefficient occurs between $p_i/p_\infty = 2{\cdot}25$ and 2·5. Further rise in the mass flow rate will not produce a reduction in *SPL* and mean pressure drag coefficient.

ACKNOWLEDGMENTS

The authors wish to thank D. G. Mabey for his suggestion on the ramp study. This work is supported by DERA under contract number WSF/U1961.

REFERENCES

1. H. Heller, D. G. Holmes, E. E. Covert 1971 *Journal of Sound and Vibration* **18**, 545–553. Flow-induced pressure oscillations in shallow cavities.
2. X. Zhang and J. A. Edwards *The Aeronautical Journal* **94**, 355–364. An investigation of supersonic oscillatory cavity flow driven by thick shear layers.
3. K. K. Ahuja and J. Mendoza 1995 *NASA CR*-4653. Effects of cavity dimensions, boundary layer, and temperature on cavity noise with emphasis on benchmark data to validate computational aeroacoustics.
4. F. Wilcox, Jr., *AIAA Journal* **26**, 374–376. Passive venting system for modifying cavity flowfields at supersonic speeds.

5. V. Sarohia and P. F. Massier 1977 *Journal of Aircraft* **14**, 833–877. Control of cavity noise.
6. L. Shaw 1982 *AIAA Paper* 82-0329. Full scale flight evaluation of suppression concepts for flow-induced fluctuating pressure in cavities.
7. H. H. Heller and D. Bliss 1975 *AIAA Paper* 75–491. The physical mechanisms of flow-induced pressure fluctuations in cavities and concepts for their suppression.
8. E. Rossiter 1964 *ARC R&M No*. 3438. Wind tunnel experiments on the flow over rectangular cavities at subsonic and transonic speeds.
9. A. Valili and C. Gauthier 1991 *AIAA Paper* 91-1645. Control of cavity flow by upstream mass injection.
10. M. E. Franke and D. L. Carr 1975 *AIAA Paper* 75-0492. Effect of geometry on open cavity flow induced pressure oscillation.
11. J. C. F. Pereira and J. M. Sousa 1994 *AIAA Journal* **32**, 1737–1740. Influence of impingement edge geometry on cavity flow oscillation.
12. D. G. Mabey 1995 Private communication.
13. X. Zhang, A. Rona and J. A. Edwards 1998 *Journal of Sound and Vibration* (to appear). An observation of pressure waves around a shallow cavity.
14. X. Zhang 1995 *AIAA Journal* **33**, 1404–1411. Compressible cavity flow oscillation due to shear layer instabilities and pressure feedback.
15. D. C. Wilcox 1988 *AIAA Journal* **26**, 1299–1310. Reassessment of the scale determining equation for advanced turbulence models.
16. M. Manna 1992 *Ph.D. Thesis*, *Université Catholique de Louvain*. A three dimensional high resolution compressible flow solver.
17. Y. N. Jeng and U. J. Payne 1995 *Journal of Aircraft* **32**, 363–369. Numerical study of a supersonic open cavity flow and pressure oscillation control.
18. H. Heller and J. Delfs 1996 *Journal of Sound and Vibration* **196**, 248–252. Cavity pressure oscillations: the generating mechanism visualized.
19. D. S. Jones 1975 *Journal of Institute of Mathematics and its Applications* **15**, 33–57. The scattering of sound by a vortex sheet.

APPENDIX: NOMENCLATURE

C_d	mean pressure drag coefficient
D	depth of cavity
f	frequency of dominant mode of oscillation
h	height of leading edge ramp and surface
M	Mach number
p	pressure
q	$\rho_\infty u_\infty^2/2$
Re	Reynolds number $\rho_\infty u_\infty D/\mu_\infty$
SPL	sound pressure level in dB, $20 \log (P_{rms}/10\ \mu\text{Pa})$
St	Strouhal number, fD/u_∞
u	streamwise velocity
v	transverse velocity
x, y	Cartesian co-ordinates
δ	thickness of boundary layer
μ	molecular viscosity
ω	specific dissipation rate
ρ	density
σ	geometric porosity

$\langle \rho v \rangle$ mass flow rate, $\int_{-D}^{0} \rho v/(\rho_\infty u_\infty)\, \mathrm{d}x/D$
$(\,)_{down}$ downstream face of cavity
$(\,)_{exp}$ expansion surface
$(\,)_i$ back wall condition
$(\,)_{ramp}$ ramp
$(\,)_{up}$ upstream face of cavity
$(\,)_w$ wall condition
$(\,)_\infty$ free stream condition